# *Turbulent Kinetic Energy in Submerged Model Canopies Under Oscillatory Flow*



**Citation:** Zhang, Yinghao et al. "Turbulent Kinetic Energy in Submerged Model Canopies Under Oscillatory Flow." Water Resources Research 54, 3 (March 2018): 1734–1750 © 2018 American Geophysical Union

**As Published:** http://dx.doi.org/10.1002/2017WR021732

**Publisher:** American Geophysical Union (AGU)

**Persistent URL:** http://hdl.handle.net/1721.1/119447

**Version:** Final published version: final published article, as it appeared in a journal, conference proceedings, or other formally published context

AGU PUBLICATIONS

Water Resources Research

RESEARCH ARTICLE
10.1002/2017WR021732

**Key Points:**
- Shedding of eddies from plants can enhance near-bed turbulence
- The contribution of plant-generated turbulence was significant when the wave excursion was greater than the stem spacing
- A canopy turbulence model developed for unidirectional flow was modified to predict turbulence intensity in oscillatory flow from wave and vegetation parameters

**Correspondence to:**
Y. Zhang,
chinayinghao@126.com

**Citation:**
Zhang, Y., Tang, C., & Nepf, H. (2018). Turbulent kinetic energy in submerged model canopies under oscillatory flow. *Water Resources Research*, *54*. https://doi.org/10.1002/2017WR021732

Received 22 AUG 2017
Accepted 17 FEB 2018
Accepted article online 22 FEB 2018



# Turbulent Kinetic Energy in Submerged Model Canopies Under Oscillatory Flow

**Yinghao Zhang[1,2,3], Caihong Tang[1,4], and Heidi Nepf[1]**

[1]Department of Civil and Environmental Engineering, Massachusetts Institute of Technology, Cambridge, Massachusetts, USA, [2]Key Laboratory of Watershed Geographic Sciences and State Key Laboratory of Lake Science and Environment, Nanjing Institute of Geography and Limnology, Chinese Academy of Sciences, Nanjing, China, [3]University of Chinese Academy of Sciences, Beijing, China, [4]Ministry of Education Key Laboratory of Water and Sediment Science, School of Environment, Beijing Normal University, Beijing, China

**Abstract** Laboratory experiments measured the velocity inside a model meadow of submerged, flexible vegetation under 1 and 2 s period waves. The model plant consisted of a rigid stem and strap-like blades, similar to the seagrass *Zostera marina* and the freshwater eelgrass *Vallisneria Americana*. The ratio of wave excursion ($A_w$) to stem spacing ($S$) determined whether, or not, plant-generated turbulence enhanced the turbulence level within the meadow, compared to bare bed. Specifically, near-bed turbulence was enhanced for conditions with $A_w/S > 0.5$, and for these conditions the turbulence (*TKE*) normalized by the RMS wave velocity squared, $TKE/U_{w,RMS}^2$, increased monotonically with the plant solid volume fraction, $\phi$. The plant-generated turbulence was greater in the stem region than in the blade region, and this was attributed to the greater relative motion between the waves and rigid stem, compared to the flexible blades. A model previously developed to predict *TKE* in unidirectional flow through a rigid emergent canopy was modified by replacing the time-mean current with the RMS wave velocity. With a fitted scale coefficient, the modified model predicts *TKE* as a function of RMS wave velocity in the meadow, stem and blade geometry, and solid volume fraction. Wave decay was also measured and shown to have a linear correlation with the measured *TKE* within the canopy, providing a second method to predict meadow *TKE* in the field.

## 1. Introduction

Freshwater and saltwater vegetation provide a wide range of ecosystem services. Aquatic vegetation protects shorelines by damping waves and storm surge, inhibits erosion by stabilizing the bed, shelters economically important fish, and enhances local water quality (e.g., Barbier et al., 2011; Costanza et al., 1997). In lakes, rivers and coastal regions, macrophytes are a foundation of the food web and promote biodiversity by creating varied habitat (e.g., Green & Short, 2003; Kemp et al., 2000). Aquatic vegetation also provides significant carbon storage (e.g., Fourqurean et al., 2012; Greiner et al., 2013). Many of these ecosystem services depend on changes in water motion associated with the vegetation. For example, by decreasing the near-bed velocity, aquatic vegetation promotes the retention of suspended particles (Fonseca & Fisher, 1986; Gleason et al., 1979; Granata et al., 2001). The retention of particles within vegetated regions can impact nutrient and contaminant cycling, as well as carbon sequestration (Kennedy et al., 2010; Luettich et al., 1990; Wang et al., 2015). Nutrient uptake by submerged vegetation is also a function of local current and wave velocity (Koch, 1994; Lei & Nepf, 2016; Thomas et al., 2000; Weitzman et al., 2013), both of which are influenced by the blade density within the meadow (Ghisalberti & Nepf, 2002; Lowe et al., 2005).

Submerged vegetation is often present in shallow aquatic systems, and its presence promotes clear water conditions, while its absence is often associated with turbid water (e.g., Hauxwell et al., 2004; Weisner & Strand, 2002). Vegetation of sufficient density can help to maintain clear water conditions by reducing resuspension (Moore, 2004). Further, because sediments can be a repository for nutrients and contaminants, wave-driven resuspension is also the main driver in nutrient and pollutant cycling in lakes (e.g., Bailey & Hamilton, 1997; Luettich et al., 1990; Wang et al., 2015). For example, the nutrient-rich sediment in Taihu Lake, China, is easily resuspended by wind-waves, and this resuspension impacts water transparency, underwater light climate, and primary production (Qin et al., 2004; Zhang et al., 2014; Zhu et al., 2005, 2015). Because wave-driven resuspension can be a key factor determining the nutrient and light levels within lakes

and coastal zones, and submerged vegetation is a common feature in these shallow water environments, we need to understand the interaction between waves and vegetation.

Several previous studies have shown that submerged vegetation can dissipate wave energy (e.g., Bradley & Houser, 2009; Luhar et al., 2017; Mendez & Losada, 2004), and, for dense meadows, diminish wave orbital velocity (Abdolahpour et al., 2017; Lowe et al., 2005; Luhar et al., 2010). The interaction between the meadow and waves can also generate a mean current in the direction of wave propagation (e.g., Abdolahpour et al., 2017; Luhar et al., 2010). Previous studies have demonstrated that flow-vegetation interaction can be a significant source of turbulence within a canopy (e.g., Banerjee et al., 2015; Nepf, 1999; Tanino & Nepf, 2008; Tse et al., 2016). Stem-generated turbulence has been shown to play a role in sediment mobilization under both unidirectional current (Yang et al., 2016) and oscillatory flow (Tinoco & Coco, 2014). A better understanding of the turbulence within submerged meadows could thus improve the prediction of sediment mobilization. Pujol et al. (2010) observed that both rigid and flexible meadows sheltered the bed from turbulence generated above the meadow using an oscillating grid in still water. The meadows reduced the near-bed turbulent kinetic energy (*TKE*) by as much as 60% relative to bare-bed conditions. The damping was enhanced by a decrease in stem diameter and an increase in stem density. Pujol and Nepf (2012) considered how a submerged meadow impacted the *TKE* generated by a breaking wave. After the breaking event, the *TKE* dissipated more rapidly above a meadow, compared to a bare channel, and this was attributed to the damping influence of the meadow. However, *TKE* measured near the bed was roughly twice as high with vegetation as without. The enhancement of *TKE* by the meadow was attributed to the generation of turbulence within the wakes of individual stems by the wave orbital velocity. Pujol et al. (2013) and Ros et al. (2014) studied small amplitude progressive waves over rigid and flexible canopy models and real vegetation (*Ruppia maritima*), and they observed that *TKE* was generally elevated within rigid canopies and diminished within flexible canopies, relative to a bare bed. However, in all cases, the wave excursion (radius of the wave orbital motion) was comparable to or smaller than the stem spacing, indicating conditions with weak wave-plant interaction (see discussion in Lowe et al., 2005). To complement the previous work, the present study considered wave excursions both smaller and larger than the stem spacing to explore conditions with both weak and strong wave-plant interaction.

While previous studies have provided useful measurements, none have proposed models to predict *TKE* within a submerged meadow under wave conditions. In this study, a model for *TKE* proposed and validated for unidirectional current through a rigid emergent canopy (Tanino & Nepf, 2008, hereafter referred to as TN08) was adapted for wave conditions within a flexible canopy. Within a canopy, vortex generation by individual stems drains energy from the mean flow and converts it to turbulent kinetic energy, so that the rate at which turbulent energy is produced by stem wakes (wake production) is proportional to the rate at which mean flow energy is extracted by canopy drag (e.g., Raupach & Shaw, 1982). Within a rigid emergent canopy exposed to unidirectional flow, the turbulent kinetic energy budget reduces to a balance between wake production and viscous dissipation (TN08). The rate of viscous dissipation can be represented with the classic scaling, $k_t^{3/2}/l_t$, in which $k_t$ is the turbulent kinetic energy, and $l_t$ is the characteristic eddy length-scale (Tennekes & Lumley, 1972). Equating the rates of viscous dissipation and wake production, the turbulence intensity within a canopy of rigid stems of diameter $d$ is (equation (2.9) in TN08)

$$\left\langle \frac{\sqrt{k_t}}{\langle \bar{u} \rangle} \right\rangle = \delta \left[ C_D \frac{l_t}{d} \frac{md^2}{2(1-\phi)} \right]^{\frac{1}{3}}. \tag{1}$$

Here $u$ is the streamwise velocity, $C_D$ is the drag coefficient, $\phi$ is the solid volume fraction, $m$ is the stem density (stems per bed area), and $\delta$ is a scale factor. The overbar, $\bar{}$, denotes the temporal averaging operation with a time interval much longer than the time scales of turbulent fluctuation and vortex shedding. The spatial averaging operation, denoted by $\langle\ \rangle$, is defined with an averaging volume that extends over many plants in the horizontal plane, but has infinitesimal thickness in the vertical. For unidirectional current through a rigid emergent canopy of circular cylinders (stems), TN08 identified two regimes defined by the relative size of the stem diameter ($d$) and spacing between stems ($S$). For $S > 2d$, $\delta = 1.1$ and $l_t = d$. For $S < 2d$, $\delta = 0.88$ and $l_t = S$. A goal of this study was to explore whether a modified version of the TN08 model could be used to predict turbulence level within a submerged flexible canopy exposed to oscillatory flow. In particular, this study included conditions with wave excursion both smaller and larger than the stem spacing, to explore conditions with both weak and strong wave-plant interaction. The experimental setup and analytical methods are described in section 2. Section 3 describes the velocity and turbulence

measurements, making comparisons between conditions with and without (bare bed) a meadow. The turbulence levels in the stem and blade regions are separately compared to the modified TN08 model. Finally, *TKE* within the meadow is correlated with measured wave energy dissipation.

## 2. Materials and Methods

The experiments were conducted in a 24 m long, 38 cm wide, and 60 cm deep flume (Figure 1) in the Nepf Lab at MIT. Waves were generated by a hydraulically driven, paddle wave maker, which was controlled by a Syscomp WGM-101 arbitrary waveform generator programmed to produce surface waves of a desired amplitude and frequency based on the closed-form solution for paddle motion described in Madsen (1971). To reduce wave reflection a 1:5 slope, aluminum beach covered with a 2 inch layer of rubberized coconut fiber was placed at the downstream end of the flume. The wave reflection varied with wave frequency and was between 2% and 16%.

The canopy was constructed using model plants placed in a staggered arrangement in predrilled baseboards. The model plant consisted of a rigid stem and strap-like blades, representative of the seagrass *Zostera marina* and the freshwater eelgrass *Vallisneria Americana*. The dynamic and geometric similarities of this model to real grasses have been described in Ghisalberti and Nepf (2002). Each model plant consisted of six blades of 14 cm length attached with waterproof tape to a 1.7 cm long wooden cylinder with 1 cm overlap. With the tape, the stem diameter was $d = 0.69 \pm 0.02$ cm. Once attached, the free blade length was $l_b = 13$ cm. The blade width was $w_b = 3$ mm and thickness was $t_b = 0.1$ mm. When inserted into the baseboard, the rigid stem (cylinder) extended 1 cm above the bed.

We considered four stem densities and cases with no canopy, matching as closely as possible the same set of wave conditions. The cases are summarized in Table 1. The S-series has no canopy. Series A, B, C, and D have increasing stem density ($m = 280$, 600, 820, and 1,370 stems/m$^2$, respectively) and include cases with $A_w/S >$ and $< 1$. With six blades per stem, these corresponded to frontal area per canopy volume $a_f$ ($= 6mw_b$) varying from 0.05 to 0.25 cm$^{-1}$, and frontal area index $a_f l_b = 0.7$ to 3.3, which fell within the range observed in the field, $a_f l_b = 0.3$ to 4, as described in Luhar et al. (2017). Wave period ($T = 1$ and 2 s), wave amplitude ($a = 1.0$ to 4.2 cm), and water depth ($h = 0.40$ to 0.45 m) were chosen to represent shallow water regions with locally wind-driven waves (see discussion in Luhar et al. (2017)).

For velocity measurements, the model canopy was 2 m long and 0.38 m wide and was located 9.5 m downstream of the wave maker (Figure 1a). A 2 m meadow was selected so that the same wave conditions could

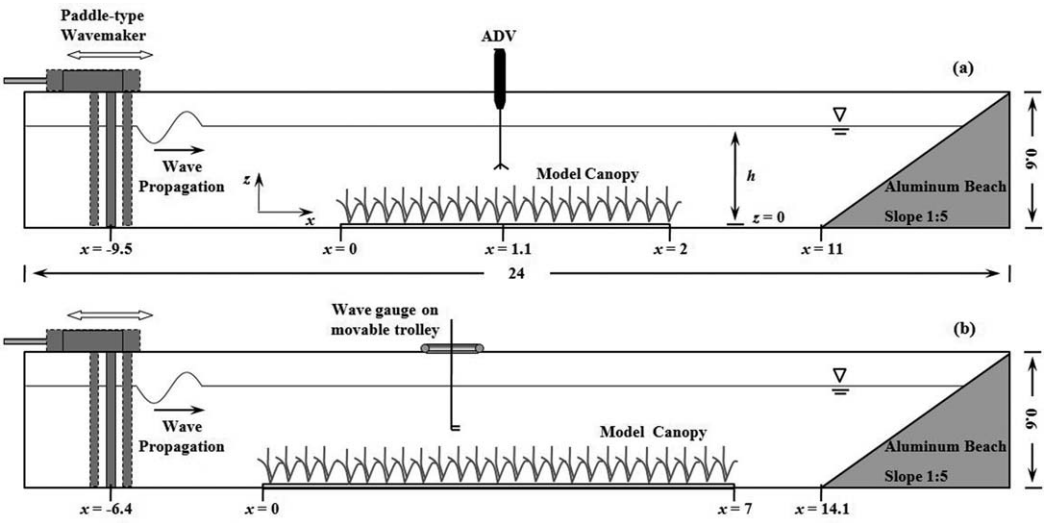


**Figure 1.** Experimental setup for (a) velocity measurements and (b) wave decay measurements. Dimensions are in meters, but not to scale. The wave maker and aluminum beach were located at the upstream and downstream end of the flume, respectively. A Nortek Vectrino measured velocity midway along the model canopy. The wave gauge was mounted on a mobile trolley and measured the water surface displacement at intervals of 10 cm over the entire length of the canopy.

**Table 1**
*Vegetation and Wave Parameters for Each Experimental Scenario*

| Run | $m$ ($m^{-2}$) | $\phi_s$[a] (%) | $\phi_b$[b] (%) | $h$ (cm) | $h_{dmax}$ (cm) | $T$ (s) | $Re$[c] | $KC$[d] | $a$[e] (cm) | $A_w$[f] (cm) | $A_w/S$[g] |
|---|---|---|---|---|---|---|---|---|---|---|---|
| S1 | 0 | | | 40 | | 2.0 | | | 1.3 | 1.9 | |
| S2 | 0 | | | 40 | | 2.0 | | | 1.5 | 2.4 | |
| S3 | 0 | | | 40 | | 2.0 | | | 2.1 | 3.0 | |
| S4 | 0 | | | 40 | | 2.0 | | | 2.4 | 3.9 | |
| S5 | 0 | | | 40 | | 2.0 | | | 3.1 | 4.5 | |
| S6 | 0 | | | 40 | | 2.0 | | | 3.2 | 5.2 | |
| S7 | 0 | | | 45 | | 1.0 | | | 1.7 | 0.6 | |
| S8 | 0 | | | 45 | | 1.0 | | | 3.5 | 1.1 | |
| A1 | 280 | 1.05 | 0.05 | 40 | 12 | 2.0 | 247 | 15 | 1.4 | 1.7 | 0.29 |
| A2 | 280 | 1.05 | 0.08 | 40 | 8 | 2.0 | 353 | 23 | 1.8 | 2.5 | 0.42 |
| A3 | 280 | 1.05 | 0.08 | 40 | 8 | 2.0 | 443 | 28 | 2.1 | 3.1 | 0.52 |
| A4 | 280 | 1.05 | 0.09 | 40 | 7 | 2.0 | 555 | 35 | 2.7 | 4.0 | 0.67 |
| A5 | 280 | 1.05 | 0.09 | 40 | 7 | 2.0 | 661 | 45 | 3.2 | 5.0 | 0.84 |
| A6 | 280 | 1.05 | 0.11 | 40 | 6 | 2.0 | 756 | 50 | 3.9 | 5.7 | 0.95 |
| A7 | 280 | 1.05 | 0.05 | 45 | 14 | 1.0 | 165 | 8 | 1.7 | 1.1 | 0.18 |
| B1[h] | 600 | 2.24 | 0.12 | 40 | 12 | 2.0 | 250 | 15 | 1.4 | 1.7 | 0.42 |
| B2[h] | 600 | 2.24 | 0.18 | 40 | 8 | 2.0 | 355 | 23 | 1.8 | 2.5 | 0.61 |
| B3[h] | 600 | 2.24 | 0.20 | 40 | 7 | 2.0 | 425 | 27 | 2.3 | 3.1 | 0.76 |
| B4[h] | 600 | 2.24 | 0.23 | 40 | 6 | 2.0 | 547 | 37 | 2.9 | 4.5 | 1.11 |
| B5[h] | 600 | 2.24 | 0.28 | 40 | 5 | 2.0 | 667 | 47 | 3.3 | 5.7 | 1.40 |
| B6 | 600 | 2.24 | 0.28 | 40 | 5 | 2.0 | 744 | 54 | 4.2 | 6.7 | 1.63 |
| B7 | 600 | 2.24 | 0.10 | 45 | 14 | 1.0 | 304 | 9 | 3.4 | 1.1 | 0.26 |
| C1[i] | 820 | 3.07 | 0.16 | 40 | 12 | 2.0 | 250 | 16 | 1.2 | 1.9 | 0.53 |
| C2[i] | 820 | 3.07 | 0.27 | 40 | 7 | 2.0 | 372 | 24 | 1.8 | 2.9 | 0.82 |
| C3[i] | 820 | 3.07 | 0.27 | 40 | 7 | 2.0 | 467 | 30 | 2.2 | 3.6 | 1.03 |
| C4[i] | 820 | 3.07 | 0.32 | 40 | 6 | 2.0 | 608 | 41 | 2.7 | 4.7 | 1.36 |
| C5[i] | 820 | 3.07 | 0.38 | 40 | 5 | 2.0 | 729 | 52 | 3.2 | 6.2 | 1.77 |
| C6[i] | 820 | 3.07 | 0.38 | 40 | 5 | 2.0 | 813 | 60 | 3.7 | 7.1 | 2.02 |
| C7 | 820 | 3.07 | 0.38 | 40 | 5 | 2.0 | 754 | 55 | 3.5 | 7.0 | 2.00 |
| C8 | 820 | 3.07 | 0.14 | 45 | 14 | 1.0 | 161 | 5 | 1.7 | 0.6 | 0.18 |
| C9 | 820 | 3.07 | 0.14 | 45 | 14 | 1.0 | 301 | 9 | 3.4 | 1.1 | 0.33 |
| D1 | 1,370 | 5.12 | 0.32 | 40 | 11 | 2.0 | 218 | 14 | 1.0 | 1.6 | 0.58 |
| D2 | 1,370 | 5.12 | 0.46 | 40 | 7 | 2.0 | 308 | 20 | 1.5 | 2.4 | 0.88 |
| D3 | 1,370 | 5.12 | 0.53 | 40 | 6 | 2.0 | 399 | 26 | 1.9 | 3.2 | 1.18 |
| D4 | 1,370 | 5.12 | 0.53 | 40 | 6 | 2.0 | 497 | 35 | 2.4 | 4.3 | 1.59 |
| D5 | 1,370 | 5.12 | 0.64 | 40 | 5 | 2.0 | 614 | 45 | 2.8 | 5.4 | 2.00 |
| D6 | 1,370 | 5.12 | 0.64 | 40 | 5 | 2.0 | 722 | 56 | 3.3 | 6.9 | 2.54 |
| | | (0.02) | (0.02) | (0.2) | (0.5) | (0.03) | | | (0.1) | (0.2) | |

Note. The values in the last row indicate experimental uncertainty.
[a]Solid volume fraction in stem region $\phi_s = m\pi d^2/4$. [b]Solid volume fraction in blade region $\phi_b = 6ml_bw_bt_b/h_{dmax}$, with $h_{dmax}$ the maximum deflected height of canopy. [c]Reynolds number in stem region, $Re = U_{w,RMS}d/\nu$, with $U_{w,RMS}$ measured at $z = 1.3$ cm. [d]Keulegan-Carpenter number estimated as $KC = (U_{max} - U_c)T/d$, in which $U_{max}$ is the maximum velocity in wave cycle measured at $z = 1.3$ cm. [e]Wave amplitude calculated by fitting linear wave (equation (5)) to measured $U_{w,RMS}$ at $z \geq 21$ cm. [f]Wave orbital excursion, $A_w = U_{max}T/(2\pi)$, the radius of wave orbital motion. [g]For regular arrays the mean center-to-center stem spacing is $S = m^{-1/2}$. [h]Wave decay over 7 m canopy measured for these cases. [i]Blade motion recorded for these cases.

be generated at the midmeadow measurement point for all meadow densities, without the need to tune the wave maker to offset the impact of wave decay. Instantaneous velocities ($u$, $v$, $w$) corresponding to the streamwise ($x$), lateral ($y$), and vertical ($z$) directions, respectively, were measured using a 3-D Acoustic Doppler Velocimeter (ADV, Nortek Vectrino) with a 200 Hz sampling rate and using a 6 min record at each measurement point. Vertical profiles of velocity were made at midway along the meadow with measurement positions at 1 cm vertical intervals from $z = 1.3$ to 25.3 cm above the bed. To keep too many blades from blocking the ADV beams, blades were removed from stems within a 5 cm radius of the measurement position, but the rigid stems were left in the boards, similar to the method described in Luhar et al. (2010). Since the blades were 13 cm long, the clearing contained some blades, just not the thickness of blades that would have been present without the clearing.

For oscillatory flow, the instantaneous velocity can be decomposed into three parts using a phase-averaging technique

$$u = U_c + U_w + u', \tag{2}$$

in which $U_c$ is the time-averaged velocity, $U_w$ is the unsteady wave velocity, and $u'$ is the turbulent velocity fluctuation, and similarly for $v$ and $w$. Spikes in the velocity record were removed using the acceleration threshold method described in Goring and Nikora (2002). The despiked velocity was segmented into individual wave periods by fitting the streamwise ($u$) velocity to a fourth-order harmonic sine curve and identifying each upward zero crossing of the velocity as the start of a wave. As a quality control, particular waves periods were selected for phase-averaging only if the measurement count within that period, $N_i$, was within 2.5% of the average measurement count for all periods ($N$). This left more than 300 and more than 150 wave periods, respectively, for the phase-average analysis of the 1 and 2 s waveforms. The phase-averaged velocity, denoted $(\tilde{u}(\varphi), \tilde{v}(\varphi), \tilde{w}(\varphi))$, was defined as the average over all periods in a given phase ($\varphi$) bin. The time-averaged velocity was calculated as:

$$U_c = \frac{1}{2\pi}\int_0^{2\pi} \tilde{u}(\varphi)d\varphi, \tag{3}$$

and similarly for $v$ and $w$. The wave velocity was defined as the root mean square (RMS) of the phase-averaged velocity, i.e.,

$$U_{w,RMS} = \sqrt{\frac{1}{2\pi}\int_0^{2\pi} (\tilde{u}(\varphi) - U_c)^2 d\varphi}. \tag{4}$$

Linear wave theory predicts

$$U_{w,RMS} = \sqrt{\frac{1}{2\pi}\int_0^{2\pi} \left(a\omega \frac{\cosh(kz)}{\sinh(kh)} \cos(kx - \omega t)\right)^2 d\varphi} = \frac{1}{\sqrt{2}} a\omega \frac{\cosh(kz)}{\sinh(kh)}, \tag{5}$$

in which $a$ is the wave amplitude, $\omega$ is the wave radian frequency, $k$ is the wave number, $h$ is the water depth, and $z$ is the vertical coordinate. The wave amplitude, $a$, was calculated by fitting the linear wave solution (equation (5)) to the measured $U_{w,RMS}$ at the highest measurement positions in the profile ($z \geq 21$ cm).

The instantaneous turbulent fluctuations were defined as the deviation of instantaneous velocity, $u$, from the phase-averaged velocity, $\tilde{u}$. The RMS fluctuations within each phase bin ($u_{rms}$, $v_{rms}$, $w_{rms}$) were used to estimate the turbulent kinetic energy in that phase bin, $1/2(u_{rms}^2 + v_{rms}^2 + w_{rms}^2)$, and the time-averaged turbulence, *TKE*, was defined as the average across all phase bins,

$$TKE = \frac{1}{4\pi}\int_0^{2\pi} \left[u_{rms}(\varphi)^2 + v_{rms}(\varphi)^2 + w_{rms}(\varphi)^2\right] d\varphi. \tag{6}$$

The noise in the ADV measurement, which could make erroneous contributions to the measured *TKE*, was determined using a measurement in still water (0.18 $cm^2/s^2$).

The wave surface displacement, $\eta(t)$, was measured at the same longitudinal position as the ADV using a wave gauge with 0.2 mm accuracy and 1,000 Hz sampling rate. The phase-averaged wave form, $\tilde{\eta}(\varphi)$, was determined using a phase-averaging method similar to that used for velocity. The variation in amplitude between individual waves, normalized by the average amplitude, $\Delta\%\eta$, estimated the contribution of amplitude variation to measured *TKE*

$$\Delta\%\eta = \frac{\frac{1}{2\pi}\int_0^{2\pi} \eta_{rms}(\varphi)d\varphi}{\eta_{w,RMS}}, \tag{7}$$

in which $\eta_{rms}(\varphi)$ was the RMS variation in surface position between individual waves within a specific phase ($\varphi$) bin, and $\eta_{w,RMS}$ was the RMS of the phase-averaged surface position, $\tilde{\eta}(\varphi)$. Based on (7), there was less than 1% variation between waves in all cases, and the contribution of this variation to the measured *TKE* ($=\sqrt{2}\,\Delta\%\eta$) was less than 1.4% of *TKE*.

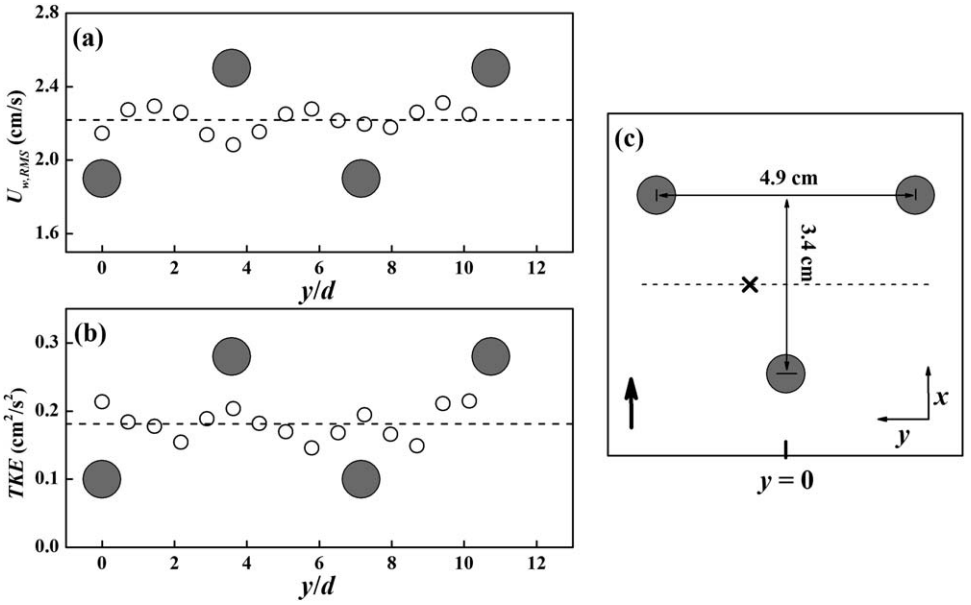


**Figure 2.** Lateral profiles of (a) $U_{w,RMS}$ and (b) *TKE* measured midway between adjacent stem rows for case B7. Velocity measured at $z = 1.3$ cm above the bed. The horizontal dashed lines in these two subplots indicate the lateral average of the measured quantity. (c) Dashed line shows position of measurement transect relative to stem rows. The heavy black arrow indicates the direction of wave propagation. The black cross (X) indicates the position at which vertical profiles were measured. The gray circles in each figure indicate stems with diameter $d = 0.69$ cm.

To assess the stem-scale variation in wave velocity within the meadow, the velocity was measured at $z = 1.3$ cm above the bed along a lateral transect (Figure 2). The lateral transect was midway between stem rows and spanned four stems. Both wave velocity and turbulence level varied with position relative to the nearest stem, with 5% and 15% deviation, respectively, from the laterally mean. Similarly, a longitudinal transect measured in the line with a stem and spanning from one stem diameter to the next stem row showed that $U_{w,RMS}$ varied by just 2% and *TKE* varied by 18% from the mean. These data suggest that under short ($\leq$2 s) wave conditions a single point measurement can be a reasonable estimate for canopy-average values. Lateral transects spanning three stems (dashed line in Figure 2c) were repeated at $z = 1.3$ cm for all cases, and vertical profiles ($z = 1.3$ to 25.3 cm) were measured at a position one-eighth the distance between two adjacent stems of the same row (marked as a cross in Figure 2c), where the local $U_{w,RMS}$ and *TKE* represent the lateral mean. Vertical profiles without the meadow (Figures 3a–3c) were also measured at the same point.

For cases C1 to C6 ($m = 820$ stems/m$^2$ and $T = 2$ s), the blade motion was captured using a Canon 80D DLSR camera. To distinguish the motion of individual blades, one of the plants midway along the meadow was constructed with black blades to contrast with the white blades in the rest of the meadow. The camera was mounted on a tripod and recorded through the side of the flume at 30 frames per second. The videos were processed in MATLAB. A trace of the blade motion over the wave cycle was constructed by summing 30 images spaced evenly over one wave period. Thresholds for the red-green-blue (RGB) pixel intensity were adjusted to enhance the contrast between the black and white blades. The blade excursion, $A_b$, at a specific vertical height was defined as the distance between the blade position at the wave crest and trough (yellow arrows shown in Figures 4a and 4d). In a separate visualization experiment, fluorescein dye was used to visualize the stem-generated turbulence. Dye was injected from a horizontal needle with its tip located 0.5 cm above the bed and just upstream of one stem. A UV light was positioned above the flume to excite the fluorescein, and the tracer trajectory was imaged through the side of the flume (Figure 5).

Wave decay was measured for the B series with $m = 600$ stems/m$^2$ (Table 1). An accurate estimate of wave decay required a meadow length of at least 1.5 wavelengths, so that for these measurements the meadow length was increased to 7 m, which corresponded to 1.9 times the wavelength $\lambda$. The leading edge of the meadow was located 6.4 m downstream of the wave maker. A wave gauge measured the water surface displacement, $\eta(x, t)$, at 10 cm intervals along the entire length of the meadow ($x = 0$ to 700 cm). At each $x$

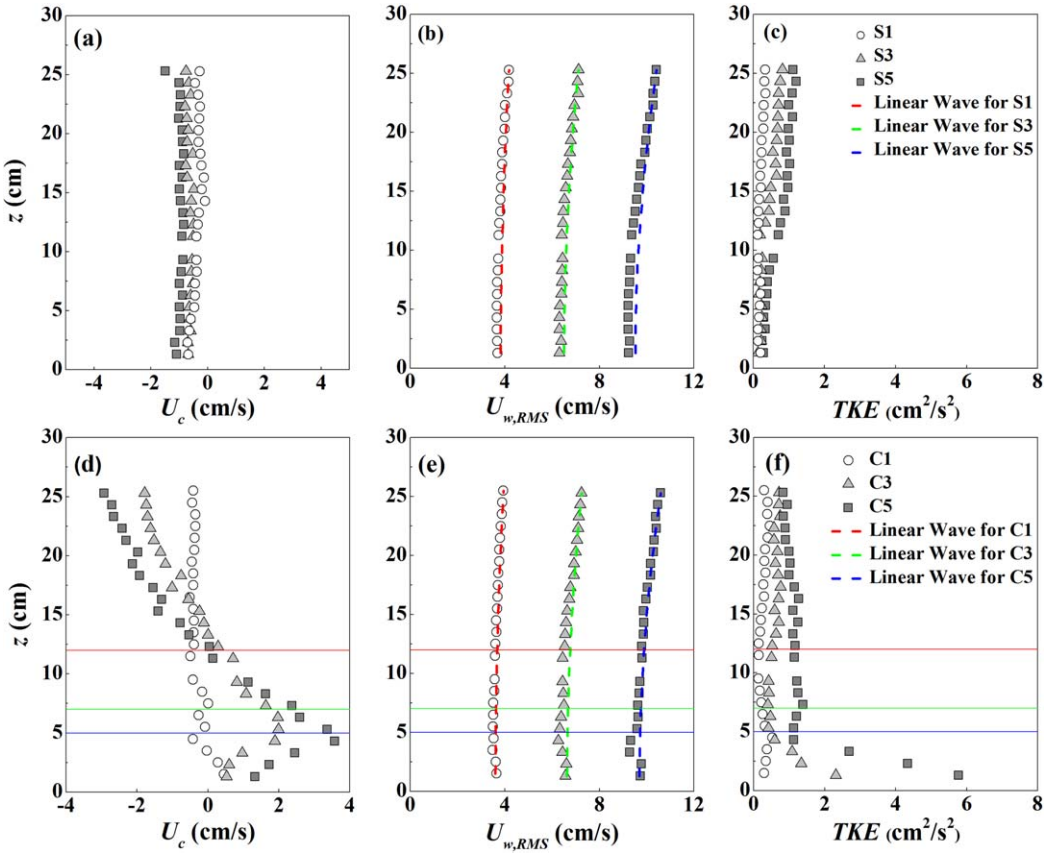


**Figure 3.** Vertical profiles of the time-mean velocity ($U_c$), RMS wave velocity ($U_{w,RMS}$), and turbulent kinetic energy (*TKE*). Subplots (a), (b), and (c) are cases with no vegetation. Subplots (d), (e), and (f) have a meadow of stem density $m = 820$ stems/m$^2$. The three meadow cases (C1, C3, and C5) have the same wave settings as the corresponding cases with a bare bed (S1, S3, and S5). The dashed lines in Figures 3b and 3e show the RMS velocity from linear wave theory. In Figures 3d, 3e, and 3f, the colored horizontal lines indicate the maximum canopy height, $h_{dmax}$, over the wave period for C1 (red), C3 (green), and C5 (blue). The weak spot of the ADV occurred at $z = 10.3$ cm, and data at this height were excluded from all profiles.

position, the water surface displacement was measured at 1,000 Hz for 60 s (30 waves), and the RMS wave amplitude, $a_{rms}$, was calculated from the RMS of the phase-averaged surface height, $\eta_{w,RMS}$, i.e.,

$$a_{rms} = \sqrt{2}\eta_{w,RMS}. \tag{8}$$

Because the waves were slightly asymmetric, there was a 10–20% difference between $a_{rms}$ and the wave amplitude, $a$, calculated by fitting the linear wave solution to the measured $U_{w,RMS}$. The wave energy dissipation rate, $E_D$, was estimated from the variation in $a_{rms}$ measured along the canopy (Dalrymple et al., 1984),

$$E_D = \frac{\partial(Ec_g)}{\rho h_{dmax}\partial x} = \frac{\partial\left(\frac{1}{2}gc_g a_{rms}{}^2\right)}{h_{dmax}\partial x}, \tag{9}$$

in which $E$ ($= {}^1/_2\rho g a_{rms}{}^2$) is the wave energy per surface area, $c_g$ ($= \lambda/T$ for shallow water waves) is the wave group velocity, which describes the propagation of wave energy, $\rho$ is the water density, $g$ is the gravity, and $h_{dmax}$ is the maximum deflected height of canopy.

## 3. Results and Discussion

### 3.1. Velocity Measurements

To set a base line, conditions without vegetation were considered first. Vertical profiles of time-mean velocity ($U_c$), RMS wave velocity ($U_{w,RMS}$), and *TKE* without vegetation are shown in Figures 3a–3c. These figures

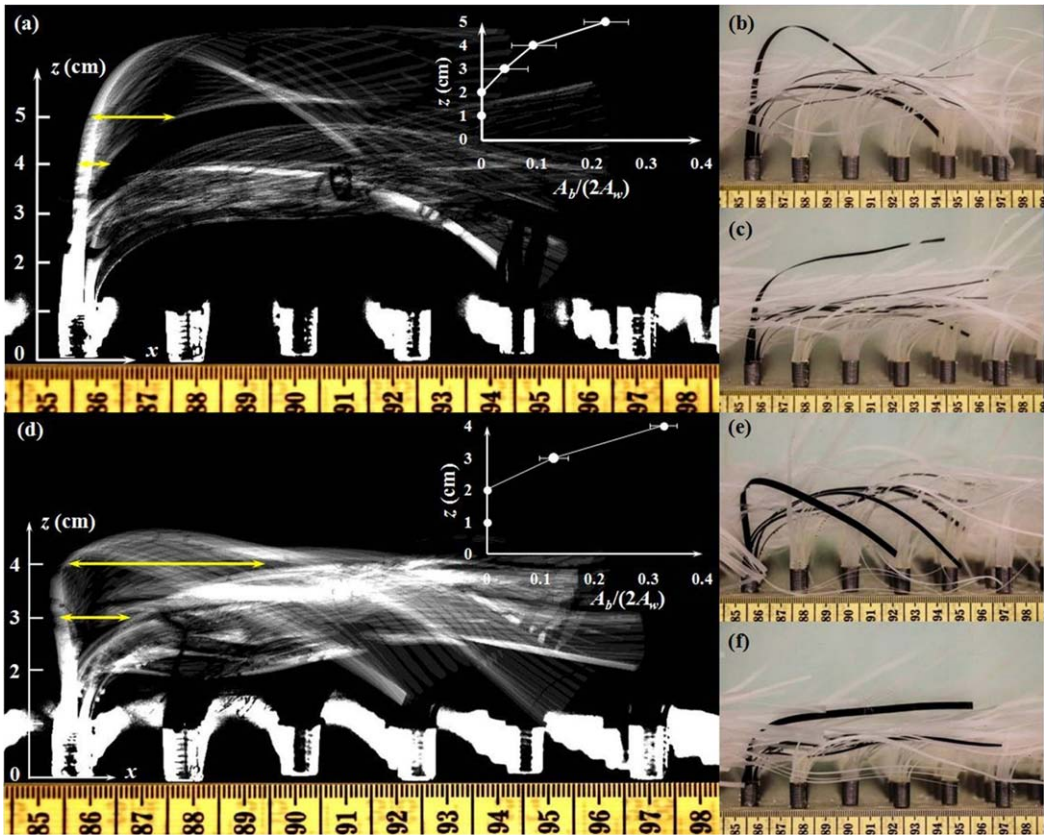


**Figure 4.** Blade posture over one wave cycle for (a, b, c) case C3, and (d, e, f) case C5. In Figures 4a and 4d, 30 images were superimposed to illustrate the blade motion over the wave cycle. A centimeter scale is shown at the bottom of each plot. The waves propagated in the positive *x* direction. The blade excursion, $A_b$, at two vertical positions is indicated with yellow horizontal arrows. The ratio of blade excursion to the diameter of wave orbital motion, $A_b/(2A_w)$, shown in inset graph, is a measure of the relative motion between the blades and water. Figures 4b and 4e show the posture occurring under the wave trough. Figures 4c and 4f show the posture under the wave crest.

compare three wave amplitudes: $a = 1.3$ cm (circle), $a = 2.1$ cm (triangle), and $a = 3.1$ cm (square), all with wave period $T = 2$ s. For each case, the time-averaged velocity was negative and vertically uniform (Figure 3a), which was consistent with a return current generated by the surface setup associated with the wave-induced Lagrangian mass flux (Fredsøe & Deigaard, 1992). The vertical distribution of RMS wave velocity followed linear wave theory to within 3.5% (dashed curves in Figure 3b). The *TKE* decreased gradually from the water surface to the bed (Figure 3c), a trend that was also observed by Pujol et al. (2010).

Figures 3d–3f show the same three wave conditions over a meadow with stem density $m = 820$ stems/m$^2$. The time-mean velocity, $U_c$, was altered by the meadow (compare Figures 3a and 3d). For the two larger amplitudes (C3 and C5), a positive mean current was generated within the meadow. As described by Luhar et al. (2010) and Abdolahpour et al. (2017), a time-mean current in the direction of wave propagation can be generated by the interaction of the wave velocity with the canopy drag. For case C1, the wave excursion, $A_w$ ($= U_{w,RMS}T/(2\pi)$), was too small to generate a significant current. As discussed in Luhar et al. (2010), the ratio of wave excursion ($A_w$) to stem spacing, $S$ ($= m^{-1/2}$), must exceed one to generate a significant mean current, whereas $A_w/S = 0.53$ for case C1. The measured RMS wave velocity followed linear wave theory above the canopy and with some reduction within the canopy. As described in Lowe et al. (2005), a reduction of wave velocity within canopy can arise from drag and inertial forces exerted by the canopy elements. For wave excursions comparable to or smaller than the stem spacing, the wave orbital velocity is reduced by the factor $\alpha = (1 - \phi)/(1 + (C_m - 1)\phi)$, with $C_m$ the added mass coefficient, which accounts for inertia that must be added to the fluid because it must be accelerated to get around the plant element. Based on a potential flow description of flow around a circular cylinder, $C_m = 2$ (Dean & Dalrymple, 1991). Measured

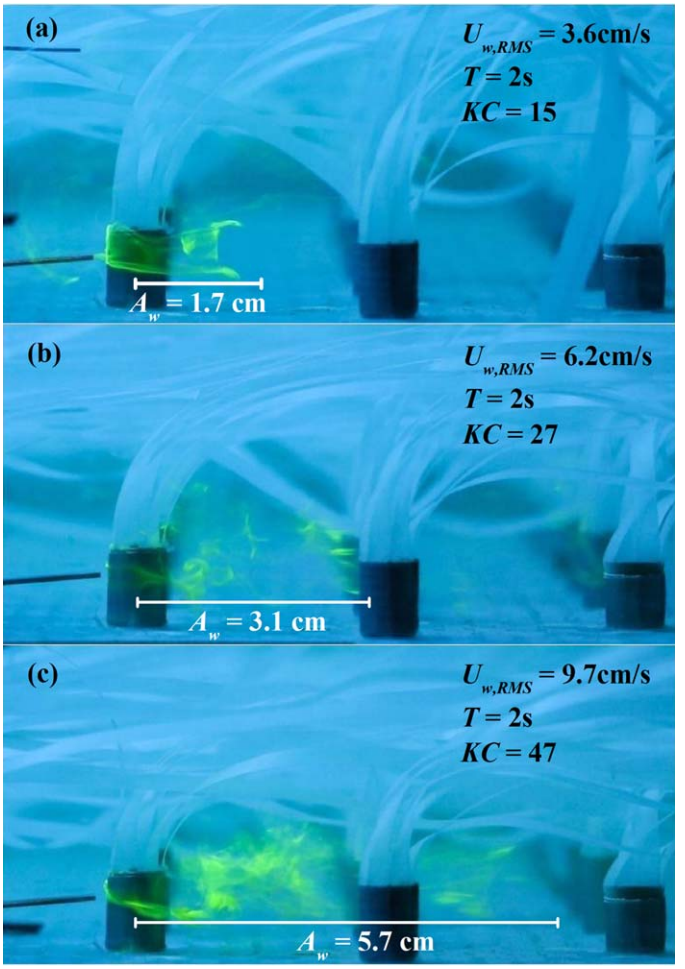


**Figure 5.** Visualization of vortices forming behind an individual stem for cases (a) B1, (b) B3, and (c) B5, with $m = 600$ stems/m$^2$. Fluorescein dye was injected from a horizontal needle visible at lower left edge of image. Waves propagated from left to right. Images were extracted from a video at the moment the blades achieved their maximum streamwise excursion. For a staggered array, stems align every other row, so the streamwise spacing between aligned stems ($S_x$) is twice the row spacing. Here $S_x = 6.8$ cm and the row spacing was 3.4 cm. The mean stem spacing $S = m^{-1/2} = 4.1$ cm.

values of $C_m$ have been shown to depend on the *KC* number, with values between 1 and 2 over the range of *KC* (= 5 to 60) present in our experiments (e.g., Keulegan & Carpenter, 1958).

Because the wave velocity responds to the local solid volume fraction, the removal of blades to allow the transit of ADV beams may impact the measured RMS wave velocity within canopy. Using the stem solid volume fraction, which is the maximum $\phi$ in the meadow, and the maximum expected $C_m = 2$, the greatest velocity reduction for the meadow density shown in Figure 3 would be $\alpha = 0.94$. That is, the removal of blades might result in a 6% overprediction of meadow wave velocity. For the highest meadow density (1,370 stems/m$^2$), the measured wave velocity was reduced by the factor $\alpha = 0.94$, which agreed with the prediction ($\alpha = 0.91$).

For cases C3 and C5, the meadow exhibited a mean pronation in the direction of wave propagation, and individual blade motion was asymmetric, with larger deflection in the direction of wave propagation. The maximum canopy height over the wave cycle, $h_{dmax}$, shown with horizontal lines in Figure 3, was 7 and 5 cm for cases C3 and C5, respectively. This was significantly less than the undisturbed canopy height (14 cm). The time-mean current likely contributed to the pronation of the meadow (Figure 3d). Equation (4) in Luhar and Nepf (2013) describes the reconfiguration of a flexible blade due to a steady current. Based on that equation, the measured maximum current, $U_{cmax} = 3.6$ and 2.0 cm/s, would produce a deflected canopy height of 10.2 and 7.1 cm in C3 and C5, respectively. These values were larger than the observed canopy heights (7 and 5 cm), indicating that deflection by the mean current did not fully explain the observed pronation. Recent numerical simulations have shown that a single flexible blade interacting with a linear wave can exhibit asymmetric blade motion, due to the contribution of the vertical wave velocity on the blade posture (see Figure 52 in Gijon Mancheno, 2016; Figures 7 and 8 in Luhar & Nepf, 2016). Since a single blade cannot generate a mean current, the blade asymmetry noted by these authors must result from the kinematics of the blade motion. In the present study, it was likely that a combination of pronation due to the mean current and asymmetric interaction between the wave and individual blades both contributed to the mean deflection of the meadow.

For the cases with a meadow, the *TKE* profile had two regions separated at roughly $z = 4$ cm (Figure 3f). Above $z = 4$ cm, *TKE* was close to being vertically uniform, and between 4 and 15 cm the *TKE* was elevated above that observed for the bare channel (Figure 3c). The *TKE* increased with wave amplitude. For $a = 1.2$, 2.2, and 3.2 cm (C1, C3, and C5), the *TKE* with a meadow was 23%, 61%, and 81% larger than the corresponding bare-bed case (S1, S3, and S5, respectively). Above $z = 15$ cm, the *TKE* was comparable in the channels with and without vegetation. Finally, in the region $z < 4$ cm within a meadow, the *TKE* increased toward the bed for the two cases with higher wave amplitudes (C3 and C5). Importantly, in this region of the meadow, the blade motion was smallest and directly at the bed the stem was completely rigid, both of which maximized the relative velocity between the plant and water. For example, Figure 4 shows blade postures for C3 and C5 over one wave cycle. The rigid stem ($z < 1$ cm) was stationary. Just above the stem, there existed a blade bundle that extended vertically about 1 cm above the stem and which also remained nearly stationary in the oscillatory flow. This part of the model plant mimics the sheath of real seagrasses, i.e., the basal region of the plant where individual blades are bundled together. Because the meadow elements were stationary in this region, the relative motion was the largest, generating strong wakes and turbulence. Above the bundled blade region, the blades moved with the wave, but over a horizontal distance smaller than the wave orbital diameter ($2A_w$). The ratio

$A_b/(2A_w)$ is an indicator for the magnitude of relative motion between the blades and water. The ratio $A_b/(2A_w)$ increased with distance from the bed (see subplots in Figures 4a and 4d), indicating decreased relative motion and thus smaller turbulence generation in the upper part of the canopy.

### 3.2. Turbulence in Stem Region

The region $z = 0$ to 2 cm will be referred to as the stem region, including the rigid stem that extended 1 cm above the bed and the bundled region of the blades, which extended roughly 1 cm above the stem. Because this region of the plant was effectively stationary (Figure 4), the wake dynamics were similar to those of a rigid cylinder in oscillatory flow, which are governed by the *Keulegan-Carpenter* number, $KC = (U_{max} - U_c)T/d$, with $U_{max}$ the maximum phase-averaged velocity (Sumer et al., 1997). For $KC < 6$, no vortex shedding will occur. Tracer visualization of fluid motion near the stem was used to demonstrate the presence of vortex shedding (Figure 5). For case B1, for which $KC = 15$, one vortex was shed by the stem in each half-period, corresponding to the single-pair regime of Sumer et al. (1997). For this case, the wave excursion ($A_w = 1.7$ cm) was smaller than the mean stem spacing ($S = m^{-1/2} = 4.1$ cm). Consistent with the small wave excursion, the shed vortex, visualized with the tracer, remained near the stem, and specifically did not cover the distance to the next downstream stem row (Figure 5a). With an increase in wave amplitude, the vortex shedding became more intense, producing greater mixing of the tracer. This is seen in case B3 ($KC = 27$) and B5 ($KC = 47$). In addition, the longer wave excursions ($A_w = 3.1$ and 5.7 cm, respectively) carried the tracer a longer distance from the stem (Figures 5b and 5c, respectively). Stem-generated turbulence can be distributed over the entire canopy when $A_w/S > \approx 1$.

Figure 6 shows the phase-averaged velocity and *TKE* as a function of phase angle, $\varphi$, measured at $z = 1.3$ cm in case C6. The stem-generated turbulence was not uniformly distributed over the wave cycle. In each half-period ($\varphi = 0°$ to 180° and $\varphi = 180°$ to 360°), there was a turbulence peak (i.e., $1/2(u_{rms}^2 + v_{rms}^2 + w_{rms}^2) > 10$ cm$^2$/s$^2$) appearing just after the maximum velocity, $\varphi = 100°$ to 160° and $\varphi = 250°$ to 300°, respectively. The turbulence peak in the first half-period (crest) was higher and of longer duration than that in the second half-period (trough). This was due to the asymmetry in the wave velocity associated with the asymmetry in wave shape, with a steeper crest and broader trough, and also to the addition of the wave-induced mean current, which enhanced the total velocity under the crest and depressed it under the trough.

In the stem region, the measured *TKE* increased with increasing wave velocity and increasing stem solid volume fraction, $\phi_s = m\pi d^2/4$ (Figure 7). Specifically, above a threshold of $U_{w,RMS}^2 \approx 20$ cm$^2$/s$^2$, *TKE* increased monotonically with the wave velocity squared, $U_{w,RMS}^2$, for each $\phi_s$ (Figure 7a). When $U_{w,RMS}^2 < 20$ cm$^2$/s$^2$, measured *TKE* was comparable to the bare-bed cases, implying that the stem wakes did not contribute significantly to near-bed turbulence under low-wave conditions. Two factors contributed to this: First, there was no vortex shedding when $KC < 6$ (Sumer et al., 1997). Second, for $KC > 6$, vortex shedding occurred, but if $A_w/S < 1$, the shed vortices remained close to the stem. The cases below the threshold $U_{w,RMS}^2 < 20$ cm$^2$/s$^2$ fell in the regime of $5 < KC < 20$ and $A_w/S < 1$. Under this range of conditions, the stem wakes did not contribute significantly to near-bed turbulence, or the contribution was isolated to a region close to the stem, due to the small wave excursion relative to stem spacing. When $U_{w,RMS}^2 > 20$ cm$^2$/s$^2$, for which the wake-generated eddies could be distributed over the full canopy volume, the linear trend between *TKE* and $U_{w,RMS}^2$ was consistent with the trend expected from TN08 model (equation (1)).

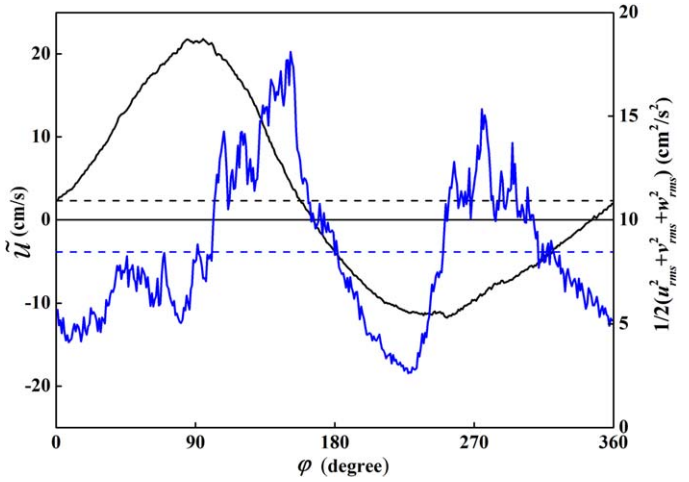


**Figure 6.** Turbulence (blue curve, right-hand axis) and velocity (black curve, left-hand axis) versus wave phase measured at $z = 1.3$ cm for case C6. The time-average *TKE* and velocity, $U_c$, are indicated by the blue and black dashed lines, respectively. The zero velocity axis is a solid black line.

To adapt the TN08 model to the oscillatory flow conditions considered here, the time-mean velocity ($\bar{u}$) was replaced by the wave velocity, $U_{w,RMS}$. In all cases considered the stem spacing, $S$, was greater than $2d$, so $l_t = d$ (TN08). With these adjustments, equation (1) can be written

$$\left\langle \frac{\sqrt{k_t}}{U_{w,RMS}} \right\rangle = \delta_1 \left[ C_D \frac{md^2}{2(1-\phi_s)} \right]^{\frac{1}{3}}, \tag{10}$$

in which $\delta_1$ was a new scale constant for the stem region under wave conditions. In oscillatory flow, $C_D$ depends on *KC*, and was chosen

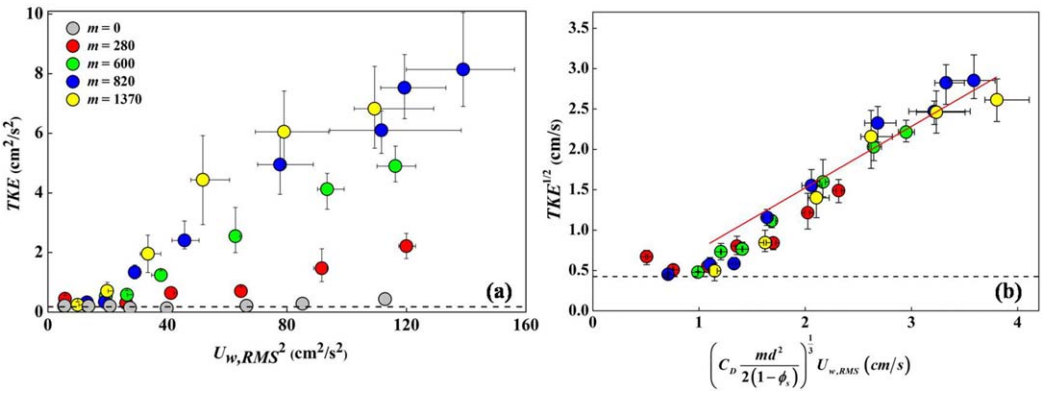


**Figure 7.** (a) Measured *TKE* plotted against the wave velocity squared, $U_{w,RMS}^2$, with measurements made in the stem region ($z = 1.3$ cm). Gray dots are bare-bed conditions. (b) $TKE^{1/2}$ measured at $z = 1.3$ cm plotted against the model prediction (equation (10)) using $U_{w,RMS}^2$ measured at $z = 1.3$ cm, assuming $\delta_1 = 1$ and $C_D = 1.4$. The red solid line indicates the best-fit line for cases with $KC \geq 20$, assuming an intercept of zero. For both figures, symbols indicate lateral averages over transect shown in Figure 2c, and error bars indicate maximum and minimum values along that transect. In some cases, the error bar was smaller than the symbol. The black, horizontal, dashed lines indicate the noise level of the ADV (0.18 $cm^2/s^2$ for Figure 7a and $0.18^{1/2} = 0.42$ cm/s for Figure 7b).

here based on previous studies of cylinders in oscillatory flow (Keulegan & Carpenter, 1958). For the cases tested in this study, *KC* varied from 5 to 60, but only conditions with $KC = 20$ to 60 produced significant near-bed turbulence (see discussion of Figure 7a). Within this range, $C_D = 1.4$ is an appropriate mean value (Keulegan & Carpenter, 1958). The scale coefficient, $\delta_1$, was determined by fitting the $TKE^{1/2}$ to $(C_D m d^2/(2(1-\phi_s)))^{1/3} U_{w,RMS}$ for cases with $KC \geq 20$, assuming an intercept of zero. As shown in Figure 7b, the best-fit line yielded $\delta_1 = 0.76 \pm 0.02$ (95% confidence limits). This was smaller than TN08's value for unidirectional current ($\delta = 1.1$). The smaller coefficient for wave conditions may be explained by the temporal variation through the wave cycle, illustrated in Figure 6.

Figure 8 shows the measured *TKE* normalized by the model $k_t$ (equation (10), with $\delta_1 = 0.76$), plotted against $A_w/S$. The observed *TKE* fit the model for $A_w/S > 1$, whereas the model overpredicted the measured turbulence for $A_w/S < 1$. For $A_w/S > 1$, the wave orbital excursions were large enough to ensure that the full canopy volume was influenced by the stem-generated turbulence (Figure 5). In contrast, when $A_w/S < 1$, only the water parcels nearest the stems interacted with stems, and for very small $A_w/S$, no vortices were generated.

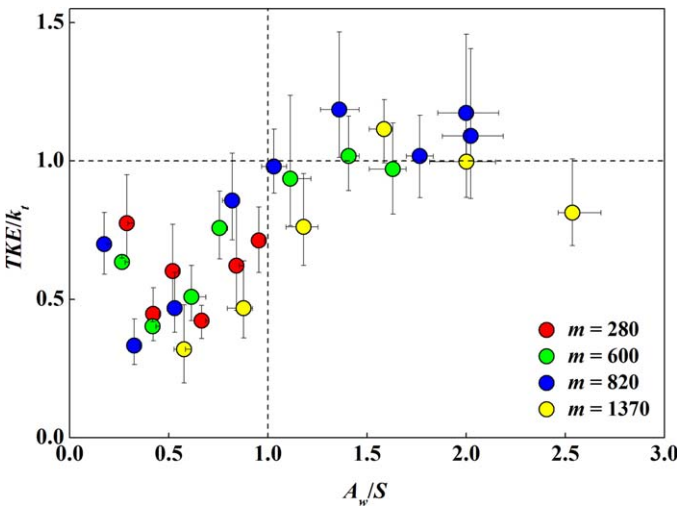


**Figure 8.** Stem-region measured *TKE* normalized by model prediction, $k_t$ (equation (10)), using the stem-region wave velocity, plotted against the ratio of wave orbital excursion to stem spacing, $A_w/S$. The stem-region velocity and *TKE* were measured at $z = 1.3$ cm. $C_D$ was assumed to be 1.4 and the scale constant $\delta_1 = 0.76$. Error bars indicate the maximum and minimum values along the lateral measurement transect shown in Figure 2c.

### 3.3. Turbulence in Blade Region

The blade region was defined from the top of the stem region to the top of the canopy, i.e., over the vertical distance $z = 2.3$ cm to the maximum deflected height of canopy ($h_{dmax}$). Over this region, the blades moved with the waves. To adapt the TN08 model to the blade region, the blade geometry must be carefully considered. First, with six blades per stem, the blade density (blades per bed area) was $m_b = 6\ m$. Second, the solid volume fraction in the blade region was $\phi_b = m_b l_b w_b t_b / h_{dmax}$. The ratio of blade length ($l_b$) to deflected canopy height ($h_{dmax}$) corrected for the compression of the blade region, which increased the solid volume fraction. Third, the blade width ($w_b$) replaced the stem diameter ($d$) as the relevant lateral dimension for the frontal area and vortex scale. Fourth, the spacing between blades was estimated as $S_b = (m_b)^{-1/2}$, which assumed erect blades, and so overestimated the spacing for the deflected canopy. $S_b$ varied from 1.1 to 2.4 cm, which was larger than $w_b$ (0.3 cm). Therefore, following the TN08 study, $l_t = w_b$ was assumed in the blade region. Applying these adjustments to equation (1)

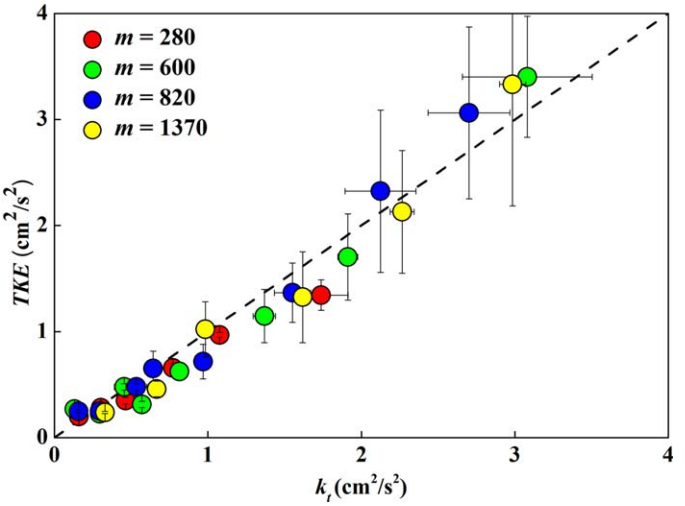


**Figure 9.** Comparison of *TKE* measured in the blade region with the model prediction, $k_t$ (equation 11), using the wave velocity measured in the blade region, $C_D = 1.95$ and $\delta_2 = 0.44$. Measured *TKE* and wave velocity were averaged from $z = 2.3$ cm to $h_{dmax}$. Error bars indicate the standard error of measured and predicted turbulence over this range.

$$\left\langle \frac{\sqrt{k_t}}{U_{w,RMS}} \right\rangle = \delta_2 \left[ C_D \frac{m_b w_b^2}{2(1-\phi_b)} \right]^{\frac{1}{3}}. \quad (11)$$

The blades had a flat geometry, similar to a rectangular slat, for which $C_D = 1.95$, as suggested by Luhar and Nepf (2016) based on Keulegan and Carpenter (1958). Scale constant in the blade region was determined to be $\delta_2 = 0.44 \pm 0.01$ (95% CI). Figure 9 compares the *TKE* measured in the blade region with the model value, $k_t$, predicted using the wave velocity measured in the blade region. The measured and modeled values fall along the 1:1 line, indicating that the turbulence model gives a good estimate of the measured *TKE*. Recall that in the stem region, the turbulence model gave a good prediction for $A_w/S > 1$, but overpredicted the measured *TKE* for $A_w/S < 1$ (Figure 8). Because the blade spacing ($S_b$) was smaller than the stem spacing ($S$), in the blade region, the ratio of wave excursion to blade spacing was greater than one ($A_w/S_b > 1$) for all cases except case B1 ($A_w/S_b = 0.7$). For this reason, the model $k_t$ was a good predictor of the measured *TKE* for all cases (Figure 9).

The model prediction assumed a single value of $C_D$ (= 1.95), based on the blade's flat geometry, and because this value produced good agreement between observed and simulated motion of a single blade (Luhar & Nepf, 2016). However, previous studies have also suggested the blade drag coefficient is a function of blade reconfiguration. For example, Houser et al. (2015) reported measured $C_D$ as a function of blade flexibility and wave properties. They provided an equation for $C_D$ as a function inverse Cauchy number, the ratio of plant rigidity to wave drag (see Figure 3 in Houser et al., 2015). We used the Houser et al. (2015) equation to explore the impact of variable $C_D$ on the *TKE* prediction. However, the inclusion of variable $C_D$ did not improve the fit. This may be because the fitted, variable $C_D$ reflects the drag on the full, reconfigured blade, whereas in the *TKE* prediction, the $C_D$ need only represent the drag on the part of the blade contributing to *TKE* production, which is the vertical component of the blade.

Finally, note that the scaling constant ($\delta$) would be different for different types of vegetation, specifically depending on the geometry and rigidity of the plant. The generation of turbulence through vortex shedding in the wake of plant elements is controlled by *KC* and *Re* (Liu & Nepf, 2016; Sumer et al., 1997). These two parameters depend on the plant geometry and its rigidity. For example, in terms of geometry, plants with thinner elements (e.g., smaller leaf or stem width) will have lower values of *Re* and *KC*, and thus require higher wave velocities to cross the threshold of vortex shedding. In terms of rigidity, more flexible plants can reduce the relative velocity between the plant elements and wave, and also reconfigure into more streamlined shapes that produce weaker wakes. Given these dependencies, one would expect that plants with thicker and stiffer blades (e.g., *Posidonia oceanica*) would have higher values of $\delta$ (producing greater *TKE* under the same wave conditions), compared to plants with thinner or more flexible blades (e.g., *Cymodocea nodosa*).

### 3.4. Importance of Wave Excursion and Stem Spacing

A comparison with data from Ros et al. (2014) further illustrates the importance of the ratio between wave excursion and stem spacing. Ros et al. (2014) considered both rigid and flexible canopies with small values of $A_w/S = 0.04$ to 0.46. T. Serra (personal communication, 2017) provided the original *TKE* measurements from Ros et al. (2014). *TKE* measured in the rigid stem region ($z = 1.3$ cm) of the present study and at $z = 5$ cm in Ros et al.'s (2014) fully rigid canopy are plotted against $A_w/S$ in Figure 10a. For $A_w/S < 0.5$, the stem-generated turbulence was comparable to the values measured for bare bed, indicated with the horizontal dashed line. The shaded region around the dashed line indicates the range of values measured for bare bed across all conditions. For $A_w/S > 0.5$ measured *TKE* increased with $A_w/S$, reaching values several times greater than the bare bed. All of the Ros et al. (2014) data fell in the range of wave conditions for which measured *TKE* within the rigid canopy were comparable to bare bed values. For the Ros et al. (2014) experiments $KC < 6$ suggesting that vortex shedding was absent, so that no augmentation from wake production was expected.

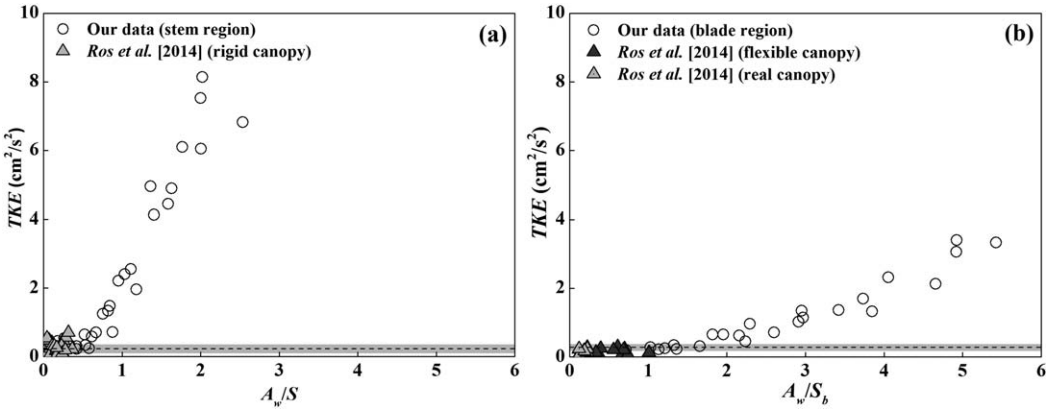


**Figure 10.** Measured *TKE* plotted against the ratio of wave excursion to stem spacing. (a) The rigid stem region in the present study and the rigid canopy in Ros et al. (2014). (b) The blade region in the present study and the flexible and real canopy (*Ruppia maritima*) in Ros et al. (2014) experiments. Ros et al. (2014) data measured at $z = 5$ cm. In each subplot, the mean (dashed horizontal line) and range (shaded region) of *TKE* measured across all bare-bed cases are shown for comparison.

Ros et al. (2014) also considered flexible and real canopies, measuring *TKE* at $z = 5$ cm, which corresponded to the blade region in our study. These data are plotted together in Figure 10b. In the Ros et al. (2014) experiments, the wave excursion was consistently smaller than the blade spacing, $S_b$, so that the contribution from wake production was expected to be small. Ros et al. (2014) noted that *TKE* was reduced for the flexible and real canopies, relative to the bare bed, and suggested that this was due to the damping of bed-generated turbulence by the vegetation. By including a wider range of wave conditions, the present study can refine this conclusion. Specifically, in the absence of a significant contribution from wake production ($A_w/S_b < 1$), the presence of a flexible canopy damps bed-generated turbulence and reduces the turbulence level within the blade region of the meadow, relative to bare-bed condition, as shown by Ros et al. (2014) and Figure 10b. However, if wake production is active ($A_w/S_b > 1$), *TKE* will be enhanced within the blade region, relative to the bare bed, as shown in Figure 10b.

### 3.5. Wave Dissipation and Turbulence Generation

Waves propagating over a canopy lose energy due to vegetation drag (e.g., Dalrymple et al., 1984), and in some cases vegetation drag is associated with turbulence generation within plant wakes (e.g., Nepf, 1999). It is therefore reasonable to expect that meadow *TKE*, if dominated by plant-wake production, will be related to the wave energy dissipation. The wave energy dissipation rate, $E_D$, was defined in equation (9). Assuming the energy dissipated from the waves was converted to turbulence within the meadow, the rate of turbulence production in the meadow ($P$) will equal the rate of wave energy dissipation ($E_D$). Further assuming that the turbulent energy locally cascades to the dissipation scale, the viscous dissipation rate ($\varepsilon$) is also equal to $E_D$. Using the viscous dissipation scaling, $\varepsilon \sim \langle k_t \rangle^{3/2} l_t^{-1}$ (Tennekes & Lumley, 1972), the turbulent kinetic energy, $k_t$, can be related to the wave decay,

$$k_t = \delta_3 (E_D l_t)^{\frac{2}{3}} = \delta_3 \left( \frac{g c_g l_t}{2 h_{dmax}} \frac{\partial a_{rms}{}^2}{\partial x} \right)^{\frac{2}{3}}. \tag{12}$$

The spatial gradient in wave amplitude, $d(a_{rms}^2)/dx$, was determined by fitting the slope of the squared amplitude, $a_{rms}{}^2$, versus distance ($x$) over the 7 m canopy. As an example, Figure 11 shows this fit for case B5. The amplitude modulation observed at half-wavelength intervals (wavelength $\lambda = 3.7$ m) was due to constructive interference with the reflected wave. The measured *TKE* is plotted versus $(E_D l_t)^{2/3}$ in Figure 12a. Three canopy regions were considered: the stem region (red circles), the blade region (green circles), and the average *TKE* over the full canopy height (blue circles). The eddy length-scale $l_t = d$ was assumed for the stem region and the canopy-average, and $l_t = w_b$ was assumed for the blade region. The maximum deflected heights $h_{dmax} = 12$, 8, 7, 6, 5 cm were used for runs B1 through B5, respectively. *TKE* increased linearly with $(E_D l_t)^{2/3}$ for each of the three regions. By fitting the slope of measured *TKE* from the stem region, blade region, and canopy-average, and assuming an intercept of zero, the scale constants were found to be

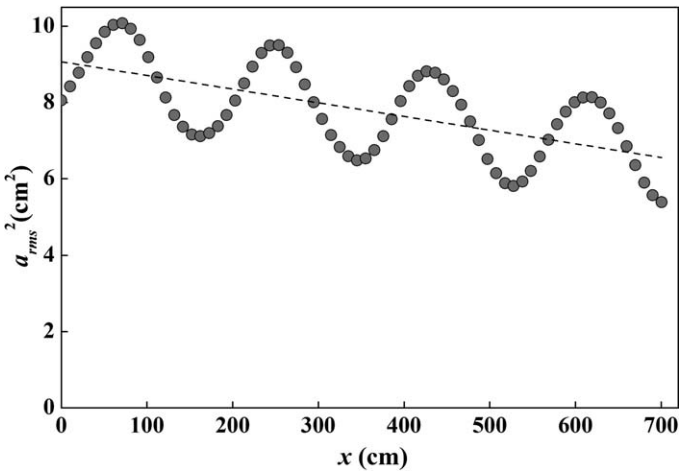


**Figure 11.** The variation in squared wave amplitude, $a_{rms}^2$, along the canopy length for case B5. $x = 0$ and 700 cm are the beginning and end of the canopy, respectively. $a_{rms}$ was calculated by equation (8). A linear fit (dashed line) was used to estimate the slope $\partial a_{\mathrm{rms}}^2/\partial x$.

$\delta_3 = 0.33 \pm 0.03$, $0.24 \pm 0.01$, and $0.24 \pm 0.02$ (95% CI), respectively. Comparison of the measured *TKE* to the predicted $k_t$ (equation (12)) is presented in Figure 12b. The turbulence was predicted well for the blade region and canopy-average. However, in the stem-region equation (12) overpredicted the measured *TKE* for the smallest waves (B1, B2, and B3). This can be explained by the ratio of wave excursion to stem spacing. For runs B4 and B5, $A_w/S > 1$, and the full stem region was influenced by the stem wakes. In contrast, for runs B1, B2, and B3, $A_w/S < 1$, and only the water near the stems was influenced by the stem wakes.

The wave dissipation method (equation (12)) for predicting meadow *TKE* more easily accommodates different morphology, because it requires less information about the meadow, i.e., only the characteristic plant length-scale, $l_t$, and the canopy deflected height, $h_{dmax}$, and it does not require estimation of a drag coefficient. However, it does require a measurement or prediction of wave decay, which may not be convenient or even possible for very short meadows. The TN08 method (equations (10) and (11)) requires more information about the canopy morphology ($m$, $\phi$, and $l_t$), as well as an estimate of drag coefficient. For both methods, the scale coefficients are dependent on plant morphology, reflecting the efficiency of energy transfer from the waves to turbulence. For plants with very fine stems and blades, the plant Reynolds number may be too small (<120, Liu & Nepf, 2016) to generate vortex shedding, in which case wave dissipation can occur with little *TKE* generation (small $\delta$). In contrast, for plants with larger stem sizes, smaller waves can surpass this limit, resulting in *TKE* generation under weaker wave conditions.

Because stem-generated turbulence has been shown to play a role in sediment mobilization (Tinoco & Coco, 2014; Yang et al., 2016), different tendencies for turbulence generation could impact meadow ecology. Meadows producing weak or no turbulence favor the deposition of fine organic matter, which augments nutrient supply for new growth, improves light climate, and facilitates carbon sequestration (Kennedy et al., 2010; Koch, 1994; Moore, 2004; Wang et al., 2015). In contrast, meadows producing strong *TKE* favor the removal of fine and organic matter, leading to a sandier substrate, which has the benefit of enhancing oxygen flux into the sediments and decreasing sulfide and ammonium levels (van Katwijk et al., 2010). As noted in section 3.3, under the same wave conditions, species with thicker and stiffer blades produce greater *TKE* than species with thinner and more flexible blades. Within a single species, meadows can

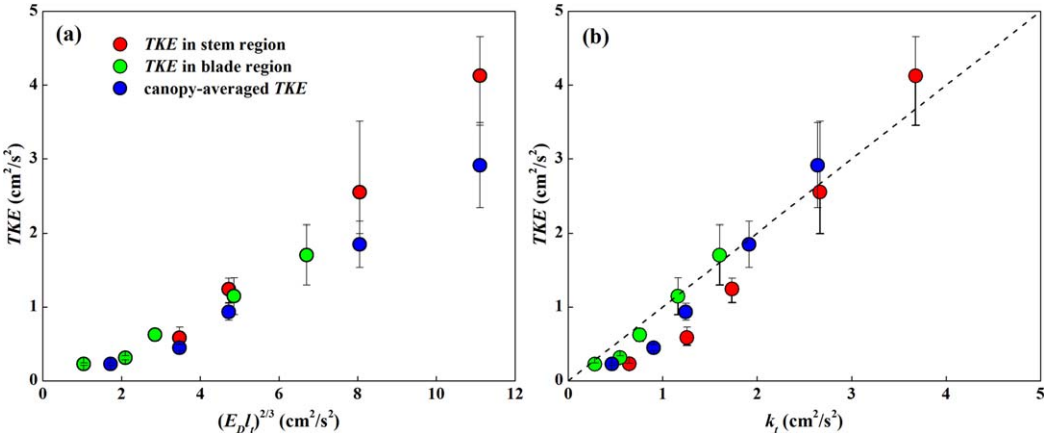


**Figure 12.** (a) Measured *TKE* plotted against $(E_D l_t)^{2/3}$ for cases B1 through B5. (b) Comparison between the measured *TKE* and the model prediction, $k_t$, from equation (12). *TKE* from three regions was considered: the stem region (measured at $z = 1.3$ cm), the blade region (averaged values over $z = 2.3$ cm to $h_{dmax}$), and the canopy-averaged *TKE* (over $z = 1.3$ cm to $h_{dmax}$). The scale constant, $\delta_3$, for each model was determined by fitting the slope of *TKE* to $(E_D l_t)^{2/3}$. The dashed line indicates $TKE = k_t$.

also adjust wave-generated *TKE* level by adjusting the shoot density ($m$ and $m_b$ in equations (10) and (11)). Finally, the area of meadow impacted by wave-generated *TKE* depends on a trade-off between wave damping and *TKE* production. More flexible meadows generate less *TKE*, but the waves and associated enhanced *TKE* persist over a longer distance into the meadow. More rigid meadows generate higher *TKE*, but the waves and *TKE* persist over shorter distance into the meadow, i.e., high levels of wave-generated turbulence at the edge of a meadow provide for the more stable, quiescent conditions at the center of a meadow. The fact that larger meadows are better able to provide this buffer region, which enhances the survival of the interior meadow, may explain why the success of seagrass restoration is correlated with meadow size (van Katwijk et al., 2016).

## 4. Conclusions

Laboratory experiments measured the velocity and turbulence (*TKE*) within a flexible canopy model under oscillatory flow. In the stem region, where the plants were stationary (or nearly so), the relative motion between the plant and water was maximized, producing the maximum turbulence within the meadow. In the stem region (or within a fully rigid canopy), above a threshold of $A_w/S = 0.5$ the turbulence was consistently greater than the bare bed, and $TKE/U_{w,RMS}{}^2$ increased monotonically with the solid volume fraction, $\phi_s = (\pi/4)md^2$. Below this threshold, $A_w/S < 0.5$, *TKE* remained comparable to the bare bed and independent of $U_{w,RMS}{}^2$ and $\phi_s$. In the blade region, blade motion decreased the relative motion between the plant and the water, producing lower *TKE* levels than observed near the bed. A turbulence model developed and validated for random arrays of rigid cylinders under unidirectional flow (TN08) was adapted to predict the *TKE* within both the stem and blade regions of the canopy. The model provided a good prediction for *TKE* in the stem and blade regions when $A_w/S$ or $A_w/S_b$, respectively, was greater than 1. Further, the *TKE* measured within the meadow was directly related to the wave energy dissipation, providing a useful tool for estimating *TKE* levels from wave decay measurements. Finally, combining the present study with results from Ros et al. (2014) provided a fuller picture of the influence of a submerged meadow on near-bed turbulence, showing that the ratio of wave excursion to stem and blade spacing plays an important role in the turbulence modulation by a canopy. In the absence of significant wake generation ($A_w/S < 0.5$, $A_w/S_b < 1$), the presence of flexible vegetation may damp bed-generated turbulence and thus reduce turbulence within the vegetation, relative to bare-bed condition. However, if wake generation is significant ($A_w/S > 0.5$, $A_w/S_b > 1$), *TKE* will be enhanced within the meadow relative to the bare bed.

**Acknowledgments**
This study received support from the U.S. National Science Foundation under grant EAR 1659923. Any conclusions or recommendations expressed in this material are those of the author(s) and do not necessarily reflect the views of the National Science Foundation. Yinghao Zhang was supported by the UCAS (UCAS[2015]37) Joint PhD Training Program and National Key Basic Research Program of China (973 Program) (2012CB417000). We sincerely thank the anonymous reviewers for providing insightful comments that have significantly improved our paper. All data necessary to evaluate and build upon the research in this paper are provided in the cited references, tables, and figures.

## References

Abdolahpour, M., Hambleton, M., & Ghisalberti, M. (2017). The wave-driven current in coastal canopies. *Journal of Geophysical Research: Oceans*, *122*, 3660–3674. https://doi.org/10.1002/2016JC012446

Bailey, M., & Hamilton, D. (1997). Wind induced sediment resuspension: A lake-wide model. *Ecological Modelling*, *99*, 217–228. https://doi.org/10.1016/S0304-3800(97)01955-8

Banerjee, T., Muste, M., & Katul, G. (2015). Flume experiments on wind induced flow in static water bodies in the presence of protruding vegetation. *Advances in Water Resources*, *76*, 11–28. https://doi.org/10.1016/j.advwatres.2014.11.010

Barbier, E., Hacker, S., Kennedy, C., Koch, E., Stier, A., & Silliman, B. (2011). The value of estuarine and coastal ecosystem services. *Ecological Monographs*, *81*(2), 169–193. https://doi.org/10.1890/10-1510.1

Bradley, K., & Houser, C. (2009). Relative velocity of seagrass blades: Implications for wave attenuation in low-energy environments. *Journal of Geophysical Research*, *114*, F01004. https://doi.org/10.1029/2007JF000951

Costanza, R., d'Arge, R., De Groot, R., Farber, S., Grasso, M., Hannon, B., et al. (1997). The value of the world's ecosystem services and natural capital. *Nature*, *387*(6630), 253–260.

Dalrymple, R., Kirby, J., & Hwang, P. (1984). Wave diffraction due to areas of energy dissipation. *Journal of Waterway Port Coastal and Ocean Engineering*, *110*(1), 67–79. https://doi.org/10.1061/(ASCE)0733-950X(1984)110:1(67)

Dean, R., & Dalrymple, R. (1991). *Water wave mechanics for engineers and scientists, Advanced series on ocean engineering* (Vol. 2). Tokyo, Japan: World Sci.

Fonseca, M., & Fisher, J. S. (1986). A comparison of canopy friction and sediment movement between four species of seagrass with reference to their ecology and restoration. *Marine Ecology Progress Series*, *29*, 15–22. https://doi.org/10.3354/meps029015

Fourqurean, J., Duarte, C., Kennedy, H., Marba, N., Holmer, M., Mateo, M., et al. (2012). Seagrass ecosystems as a globally significant carbon stock. *Nature Geoscience*, *5*(7), 505. https://doi.org/10.1038/NGEO1477

Fredsøe, J., & Deigaard, R. (1992). *Mechanics of coastal sediment transport*. Singapore: World Science.

Ghisalberti, M., & Nepf, H. (2002). Mixing layers and coherent structures in vegetated aquatic flows. *Journal of Geophysical Research*, *107*(C2). https://doi.org/10.1029/2001JC000871

Gijon Mancheno, A. (2016). *Interaction between wave hydrodynamics and flexible vegetation* (MS thesis). Delft, Netherlands: Delft University of Technology. Retrieved from http://repository.tudelft.nl/

Gleason, M., Elmer, D., Pien, N., & Fisher, J. J. (1979). Effects of stem density upon sediment retention by salt marsh cord grass, *Spartina alterniflora* Loisel. *Estuaries Coasts*, *2*(4), 271–273. https://doi.org/10.2307/1351574

Goring, D., & Nikora, V. (2002). Despiking acoustic Doppler velocimeter data. *Journal of Hydraulic Engineering*, *128*(1), 117–126. https://doi.org/10.1061/(ASCE)0733-9429(2002)128:1(117)
Granata, T., Serra, T., Colomer, J., Casamitjana, X., Duarte, C., & Gacia, E. (2001). Flow and particle distributions in a nearshore seagrass meadow before and after a storm. *Marine Ecology Progress Series*, *218*, 95–106. https://doi.org/10.3354/meps218095
Greiner, J., McGlathery, K., Gunnell, J., & McKee, B. (2013). Seagrass restoration enhances "blue carbon" sequestration in coastal waters. *PLoS One*, *8*(8), e72469. https://doi.org/10.1371/journal.pone.0072469
Green, E., & Short, F. (2003). *World atlas of seagrasses*. Berkeley, CA: University of California Press.
Hauxwell, J., Osenberg, C., & Frazer, T. (2004). Conflicting management goals: Manatees and invasive competitors inhibit restoration of a native macrophyte. *Ecological Applications*, *14*(2), 571–586. https://doi.org/10.1890/02-5250
Houser, C., Trimble, S., & Morales, B. (2015). Influence of blade flexibility on the drag coefficient of aquatic vegetation. *Estuaries Coasts*, *38*(2), 569–577. https://doi.org/10.1007/s12237-014-9840-3
Kemp, J., Harper, D., & Crosa, G. (2000). The habitat-scale ecohydraulics of rivers. *Ecological Engineering*, *16*, 17–29. https://doi.org/10.1016/S0925-8574(00)00073-2
Kennedy, H., Beggins, J., Duarte, C., Fourqurean, J., Holmer, M., Marbà, N., et al. (2010). Seagrass sediments as a global carbon sink: Isotopic constraints. *Global Biogeochemistry Cycles*, *24*, GB4026. https://doi.org/10.1029/2010GB003848
Keulegan, G., & Carpenter, L. (1958). Forces on cylinders and plates in an oscillating fluid. *Journal of Research of the National Bureau of Standards*, *60*(5), 423–440.
Koch, E. (1994). Hydrodynamics, diffusion-boundary layers and photosynthesis of the seagrasses *Thalassia testudinum* and *Cymodocea nodosa*. *Marine Biology*, *118*(4), 767–776. https://doi.org/10.1007/BF00347527
Lei, J., & Nepf, H. (2016). Impact of current speed on mass flux to a model flexible seagrass blade. *Journal of Geophysical Research: Oceans*, *121*, 4763–4776. https://doi.org/10.1002/2016JC011826
Liu, C., & Nepf, H. (2016). Sediment deposition within and around a finite patch of model vegetation over a range of channel velocity. *Water Resources Research*, *52*, 600–612. https://doi.org/10.1002/2015WR018249
Lowe, R., Koseff, J., & Monismith, S. (2005). Oscillatory flow through submerged canopies: 1. Velocity structure. *Journal of Geophysical Research*, *110*, C10016. https://doi.org/10.1029/2004JC002788
Luettich, R., Harleman, D., & Somlyody, L. (1990). Dynamic behavior of suspended sediment concentrations in a shallow lake perturbed by episodic wind events. *Limnology and Oceanography*, *35*(5), 1050–1067. https://doi.org/10.4319/lo.1990.35.5.1050
Luhar, M., Coutu, S., Infantes, E., Fox, S., & Nepf, H. (2010). Wave-induced velocities inside a model seagrass bed. *Journal of Geophysical Research*, *115*, C12005. https://doi.org/10.1029/2010JC006345
Luhar, M., Infantes, E., & Nepf, H. (2017). Seagrass blade motion under waves and its impact on wave decay. *Journal of Geophysical Research: Oceans*, *122*, 3736–3752. https://doi.org/10.1002/2017JC012731
Luhar, M., & Nepf, H. M. (2013). From the blade scale to the reach scale: A characterization of aquatic vegetative drag. *Advances in Water Resources*, *51*, 305–316. https://doi.org/10.1016/j.advwatres.2012.02.002
Luhar, M., & Nepf, H. (2016). Wave-induced dynamics of flexible blades. *Journal of Fluids and Structures*, *61*, 20–41. https://doi.org/10.1016/j.jfluidstructs.2015.11.007
Madsen, O. (1971). On the generation of long waves. *Journal of Geophysical Research*, *76*(36), 8672–8683. https://doi.org/10.1029/JC076i036p08672
Mendez, F., & Losada, I. (2004). An empirical model to estimate the propagation of random breaking and nonbreaking waves over vegetation fields. *Coastal Engineering*, *51*(2), 103–118. https://doi.org/10.1016/j.coastaleng.2003.11.003
Moore, K. A. (2004). Influence of seagrasses on water quality in shallow regions of the lower Chesapeake Bay. *Journal of Coastal Research*, *20*(Special Issue), 162–178. https://doi.org/10.2112/SI45-162.1
Nepf, H. (1999). Drag, turbulence, and diffusion in flow through emergent vegetation. *Water Resources Research*, *35*(2), 479–489. https://doi.org/10.1029/1998WR900069
Pujol, D., Casamitjana, X., Serra, T., & Colomer, J. (2010). Effect of submerged aquatic vegetation on turbulence induced by an oscillating grid. *Continental Shelf Research*, *30*, 1019–1029. https://doi.org/10.1016/j.csr.2010.02.014
Pujol, D., Casamitjana, X., Serra, T., & Colomer, J. (2013). Canopy-scale turbulence under oscillatory flow. *Continental Shelf Research*, *66*, 9–18. https://doi.org/10.1016/j.csr.2013.06.012
Pujol, D., & Nepf, H. (2012). Breaker-generated turbulence in and above a seagrass meadow. *Continental Shelf Research*, *49*, 1–9. https://doi.org/10.1016/j.csr.2012.09.004
Qin, B., Hu, W., Gao, G., Luo, L., & Zhang, J. (2004). Dynamics of sediment resuspension and the conceptual schema of nutrient release in the large shallow Lake Taihu, China. *Chinese Science Bulletin*, *49*(1), 54–64. https://doi.org/10.1007/BF02901743
Raupach, M., & Shaw, R. (1982). Averaging procedures for flow within vegetation canopies. *Boundary-Layer Meteorology*, *22*, 79–90. https://doi.org/10.1007/BF00128057
Ros, À., Colomer, J., Serra, T., Pujol, D., Soler, M., & Casamitjana, X. (2014). Experimental observations on sediment resuspension within submerged model canopies under oscillatory flow. *Continental Shelf Research*, *91*, 220–231. https://doi.org/10.1016/j.csr.2014.10.004
Sumer, B., Christiansen, N., & Fredsøe, J. (1997). The horseshoe vortex and vortex shedding around a vertical wall-mounted cylinder exposed to waves. *Journal of Fluid Mechanics*, *332*, 41–70. https://doi.org/10.1017/S0022112096003898
Tanino, Y., & Nepf, H. (2008). Lateral dispersion in random cylinder arrays at high Reynolds number. *Journal of Fluid Mechanics*, *600*, 339–371. https://doi.org/10.1017/S0022112008000505
Tennekes, H., & Lumley, J. (1972). *A first course in turbulence* (300 pp.). Cambridge, MA: MIT Press.
Thomas, F., Cornelisen, C., & Zande, J. (2000). Effects of water velocity and canopy morphology on ammonium uptake by seagrass communities. *Ecology*, *81*(10), 2704–2713. https://doi.org/10.1890/0012-9658(2000)081[2704:EOWVAC]2.0.CO;2
Tinoco, R., & Coco, G. (2014). Observations of the effect of emergent vegetation on sediment resuspension under unidirectional currents and waves. *Earth Surface Dynamics*, *2*(1), 429–483. https://doi.org/10.5194/esurf-2-83-2014
Tse, I., Poindexter, C., & Variano, E. (2016). Wind-driven water motions in wetlands with emergent vegetation. *Water Resources Research*, *52*, 2571–2581. https://doi.org/10.1002/2015WR017277
van Katwijk, M., Bos, A., Hermus, D., & Suykerbuyk, W. (2010). Sediment modification by seagrass beds: Muddification and sandification induced by plant cover and environmental conditions. *Estuarine, Coastal and Shelf Science*, *89*, 175–181. https://doi.org/10.1016/j.ecss.2010.06.008
van Katwijk, M. M., Thorhaug, A., Marba, N., Orth, R. J., Duarte, C. M., Kendrick, G. A., et al. (2016). Global analysis of seagrass restoration: The importance of large-scale planting. *Journal of Applied Ecology*, *53*, 567–578. https://doi.org/10.1111/1365-2664.12562
Wang, J., Pang, Y., Li, Y., Huang, Y., & Luo, J. (2015). Experimental study of wind-induced sediment suspension and nutrient release in Meiliang Bay of Lake Taihu, China. *Environmental Science and Pollution Research*, *22*(14), 10471–10479. https://doi.org/10.1007/s11356-015-4247-7

Weisner, S., & Strand, J. (2002). Ecology and management of plants in aquatic systems. In Perrow, M. R. & Davy, A. J. (Eds.), *Handbook of ecological restoration, Principles of restoration* (Vol. 1, p. 242). Cambridge, UK: Cambridge University Press.

Weitzman, J., Aveni-Deforge, K., Koseff, J., & Thomas, F. (2013). Uptake of dissolved inorganic nitrogen by shallow seagrass communities exposed to wave-driven unsteady flow. *Marine Ecology Progress Series*, *475*, 65. https://doi.org/10.3354/meps09965

Yang, J. Q., Chung, H., & Nepf, H. (2016). The onset of sediment transport in vegetated channels predicted by turbulent kinetic energy. *Geophysical Research Letters*, *43*, 11,261–11,268. https://doi.org/10.1002/2016GL071092

Zhang, Y., Shi, K., Liu, X., Zhou, Y., & Qin, B. (2014). Lake topography and wind waves determining seasonal-spatial dynamics of total suspended matter in turbid Lake Taihu, China: Assessment using long-term high-resolution MERIS data. *PLoS One*, *9*(5), e98055. https://doi.org/10.1371/journal.pone.0098055

Zhu, G., Qin, B., & Gao, G. (2005). Direct evidence of phosphorus outbreak release from sediment to overlying water in a large shallow lake caused by strong wind wave disturbance. *Chinese Science Bulletin*, *50*(6), 577–582. https://doi.org/10.1007/BF02897483

Zhu, M., Zhu, G., Nurminen, L., Wu, T., Deng, J., Zhang, Y., et al. (2015). The influence of macrophytes on sediment resuspension and the effect of associated nutrients in a shallow and large lake (Lake Taihu, China). *PLoS One*, *10*(6), e0127915. https://doi.org/10.1371/journal.pone.0127915